Location of Spectroscopic Probes in Self-Aggregating Assemblies. II. The Location of Pyrene and Other Probes in Sodium Dodecyl Sulfate Micelles

Nataly Lebedeva,† Radha Ranganathan, and Barney L. Bales*

Department of Physics and Astronomy and the Center for Supramolecular Studies, California State University at Northridge, Northridge, California 91330-8268

Received: January 22, 2007; In Final Form: March 3, 2007

The location of pyrene in sodium dodecyl sulfate (SDS) micelles is determined as a function of the aggregation number, *N*, by exploiting the fact that spin probes 5- and 16-doxyl stearic acid methyl esters (5DSE and 16DSE, respectively) are effective quenchers of pyrene fluorescence. The locations of the two spin probes are known from Part 1 of this series (*J. Phys. Chem. B* **2006**, *110*, 9791) and the distance between the probes and pyrene is determined by using a hydrodynamic theory to predict the quenching rate constant. The hydrodynamic theory requires the microviscosity of the regions through which the probe and pyrene diffuse. The same spin probe that serves as quencher provides a measure of the microviscosity; thus, all the information needed to locate pyrene is available from each spin probe. Employing 5DSE, at $N = 53$, pyrene is found to diffuse through a zone 67% of which lies within the Stern layer and 33% in the core. As the micelle grows, due to increasing either the surfactant or added-salt concentration, this diffusion zone moves outward such that, at $N = 130$, near the sphere-rod transition, it lies approximately 75% within the Stern layer and 25% in the core. Employing 16DSE, the location of pyrene is within 0.4 Å of that found from 5DSE at low values of *N* and within 0.8 Å at high values. Full information required to locate pyrene by using the currently developed method is not yet available for other spin probes and other commonly employed quenchers; nevertheless, using a variety of strategies and reasonable assumptions leads to the same location of pyrene within the uncertainties of the method. All of the spectroscopic probes employed in this study are largely located within the polar shell of the micelles, the largest departure being about 4% of the diameter of the micelle.

Introduction

This is the second in a series of papers dedicated to locating spectroscopic probes in self-assembled aggregates. Part 1[1] used a strategy that relied on the interaction of nitroxide spin probes with micelles of known structure. That was an example of an approach that we call the "probe-aggregate interaction" strategy (PAI) that is illustrated in Figure 1. The oval represents the known structure of the assembly at some moment and the circles and rectangles represent the pertinent moieties of probe molecules. Portions of the probe molecules may be silent spectroscopically; the locations of these are not available and are not shown. Suppose that the circles *A* and *B* may be located by comparing the local structure of the assembly with that sensed by the probe, i.e., the PAI is applicable. For the PAI to be effective, the probes must be sufficiently sensitive to the local structure and the local structure must change significantly over distances comparable to the aggregate size. A second approach that we develop in this paper we call the "probe−probe interaction" strategy (PPI). The PPI uses probe−probe interactions to define relative positions of two probes. The rectangle *C* represents a probe with insufficient sensitivity to the structure of the assembly to determine its location by the PAI; however, its interactions with other probes whose locations are known could allow its location to be found. The dashed rectangle

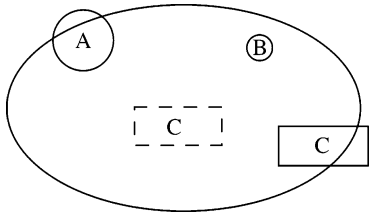

Figure 1. Schematic location of probes within an aggregate (oval) of known structure. Circles represent probes located by their interaction with the aggregate, employing the PAI. The rectangles are found by their relative positions with respect to *A* or *B*, employing the PPI. The solid and dashed rectangles are possible positions of *C* when only its interaction with *A*, for example, is employed. The ambiguity is lifted when the interaction of *C* with *B* is also exploited.

represents one of two possible locations of moiety *C* when defined by its interaction with only *A* or *B*. This ambiguity is eliminated when the rectangle's interaction with both is determined. If *A* and *B* interact sufficiently with one another, then both the PAI and the PPI are applicable, providing a consistency check on their location. The precision with which we may locate probe moieties is limited by their effective sizes, represented schematically by the size of the circles *A* and *B*. Thus, potentially, the location of *B* could be determined with higher precision than that of *A* by using the PAI and the location of *C* may be determined with more precision through its interaction with *B* than with *A*. Nevertheless, its own effective size limits our knowledge of the location of *C*. Assemblies of interest in this series of papers are dynamic structures; thus, by "location", we mean a time average.

* Address correspondence to this author. E-mail: barney.bales@csun.edu. Webpage: http://www.csun.edu/~vcphy00s/BBVita.html.

† Present address: CB# 3290, Department of Chemistry, University of North Carolina, Chapel Hill, NC 27599.

10.1021/jp070540j CCC: $37.00
Published on Web 05/09/2007

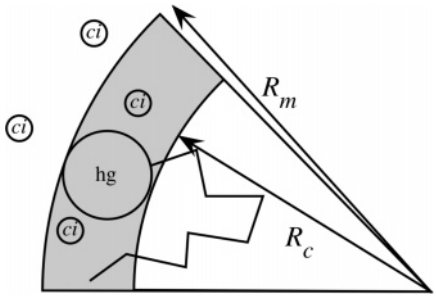

Figure 2. Schematic representation of the core−shell model of a spherical micelle showing the micelle radius, R_m, the core radius, R_c, the head groups, hg, and the counterions, ci. The volume fraction of the shell occupied by water, H_{shell}, is found by subtracting the volumes occupied by ci, hg, and any portion of the alkyl chains that resides within the shell from the volume of the shell and dividing by the volume of the shell.

Part 1[1] detailed the motivation for studies to pinpoint the location of spectroscopic probes and showed how the PAI may be employed to establish a 'benchmark" probe.[1] The reader is referred to Part 1 for details;[1] briefly, the location of the nitroxide moiety (NO•) of 5-doxyl stearic acid methyl ester (5DSE) was shown to be consistent with the zero-order model of probe location (ZOM) using the PAI in micelles formed from the sodium alkyl sulfates with chain lengths 8−12, and ammonium dodecyl sulfate.[1] 5DSE was also shown to follow the ZOM in dodecyl trimethylammonium bromide (DTAB) micelles.[2] The ZOM holds if NO• resides exclusively within the polar shell of an approximately spherical micelle while various experimental parameters are varied. Nitroxides may be located within a micelle by comparing the experimental value of the volume fraction occupied by water, *H*, with theory. The strategy is successful because not only does *H* vary rapidly as a function of the radial position of NO•, changing from zero to unity over a few angstroms, but also *H* may be measured to high precision by electron paramagnetic resonance (EPR). Part 1 also showed[1] that 16-doxyl stearic acid methyl ester (16DSE) did not conform to the ZOM in any of the micelles, showing a shifting of position inward as the micelles grew as a result of increasing the surfactant concentration or adding salt. In the scheme of Figure 1, the circles would represent the location of 5DSE and 16DSE as determined by EPR measurements of *H*. Obviously, when we find the location of NO• we remain ignorant of the location of the rest of the spin probe molecule.

One of the main objectives of this paper is to find the location of pyrene (represented by the rectangle in Figure 1) in SDS micelles. In addition, we illustrate the use of EPR and time-resolved fluorescence quenching (TRFQ) to locate other probes in SDS micelles using various combinations of the PAI and the PPI.

The scheme of Figure 1 would apply, in principle, to many probes with various spectroscopic techniques. Here we employ EPR of nitroxide probes to effect the PAI because of the excellent precision obtainable, the relatively well-defined location of the NO• moiety, and the added benefit that the microviscosity is obtainable from the same experiment. TRFQ is used to implement the PPI because the rate constant of fluorescence quenching may be measured to high precision. Pyrene was chosen for the fluorophore because it has come to dominate studies of self-assembled aggregates. The specification of the location of a given probe will be considered definitive only if it is consistent with all techniques.

Theory

Figure 2 shows a schematic of the core−shell model that we assume describes SDS micelles for all values of *N* below the sphere−rod transition near $N = 130$. By setting the volume of the core equal to the total volume of *N* hydrocarbon chains we may compute the core radius, R_c, as follows:

$$NV_{tail} = \frac{4\pi}{3} R_c^3 \tag{1}$$

In eq 1, V_{tail} is the volume (Å^3) of one chain that may be computed from the Tanford formula[3] as follows:

$$V_{tail} = 27.4 + 26.9(N_c - N_{wet}) \tag{2}$$

where $N_c = 12$ is the number of carbons in the alkyl chain and N_{wet} is the number of methylene groups residing in the polar shell. For a given value of the shell thickness, t_s, the micelle radius, $R_m = R_c + t_s$, is defined permitting the computation of the volumes of the shell and micelle as follows:

$$V_{shell} = \frac{4\pi}{3}(R_m^3 - R_c^3) \tag{3}$$

and

$$V_{micelle} = \frac{4\pi}{3} R_m^3 \tag{4}$$

The aggregation number of SDS micelles is given by[4]

$$N = N^0(C_{aq}/\mathrm{cmc}_0)^\gamma \tag{5}$$

where $N^0 = 49.5$ is the aggregation number at the cmc in the absence of added salt, cmc_0, $\gamma = 0.25$ is a constant, and C_{aq} is the concentration of counterions in the aqueous phase given by

$$C_{aq} = [\alpha C + (1 - \alpha)C_{free} + C_{ad}]/(1 - VC) \tag{6}$$

C and C_{free} are the concentrations of total SDS and of SDS in the form of monomer, respectively, and C_{ad} is the concentration of added NaCl. All concentrations in this paper are in moles per liter. *V* is the molar volume of the anhydrous surfactant and $\alpha = 0.27$[5,6] is the degree of micelle ionization. C_{free} is computed from eq 5 of ref 4. The reader is referred to recent papers where we have thoroughly discussed the computation of C_{aq} and the variation of *N*.[6−10] The ability to systematically vary *N* is an invaluable tool in these studies. Moreover, being able to produce micelles of the same size in samples containing different micelle concentrations (by maintaining C_{aq} constant, eq 6) provides a method to investigate the influence of interactions between micelles. In general, observables from spectroscopic probes are not heavily influenced by such interactions; however, in Figure 4 below, we show that sometimes they may be discerned.

From eqs 1−6, it is clear that all geometrical information is uniquely determined by the concentrations of SDS and added NaCl.

Volume Fraction of the Shell Occupied by Water. The volume fraction of the polar shell occupied by water is computed (Figure 2) by using a simple continuum model as follows:

$$H_{shell} = \frac{V_{shell} - V_{dry}}{V_{shell}} \tag{7}$$

where

$$V_{dry} = N[V_{hg} + (1 - \alpha)V_{ci} + N_{wet}V_{CH_2}] \quad (8)$$

where V_{hg}, V_{ci}, and V_{CH_2} are the volumes of a headgroup, one counterion, and one methylene group, respectively. Equations 7 and 8 apply to anionic, cationic, and nonionic (without ci) micelles. In principle, α and N_{wet} could vary with N; however, in SDS, SDS mixed with a sugar-based nonionic surfactant, ammonium dodecyl sulfate, normal sodium alkyl sulfates with chain lengths 8−11, 13, and 14, lithium dodecyl sulfate, DTAB, and dodecyl trimethylammonium chloride, both have been found to be constant.[11] For small inorganic counterions such as sodium and lithium, V_{ci} is neglected. Recall that V_{ci} is the volume of the bare ion; the waters of hydration are added to the *free* waters in computing the theoretical value of H_{shell}, detailed below.[12] For a detailed discussion of this point, see ref 13.

Spin-Probe Sensed Values of *H*. Chart 1 shows some of the nitroxide spin probes employed in this work as well as other quenchers. From the EPR spectra of spin probes, the hyperfine spacing between the low- and center-field resonances, A_+, may be measured with excellent precision.[6] Theoretically, A_+ is well understood; see, for example, refs 14−22. Mukerjee et al.[15] introduced a nonempirical polarity scale, *H*, defined to be the ratio of molar concentration of OH dipoles in a solvent or solvent mixture to that in water. For micelles containing no hydrogen-bonding moieties other than water, *H* is equal to the volume fraction occupied by water. Thus, in the shell, it is equal to eq 7. The spin-probe technique to measure *H*, which we denote by $H_{NO\bullet}$ is based on the fact that A_+ varies linearly with $H_{NO\bullet}$ as follows:

$$A_+ = A_+^0 + \frac{\partial A_+}{\partial H} H_{NO\bullet} \quad (9)$$

with constant $\partial A_+/\partial H$. Equation 9 has been calibrated for 5DSE,[23] 16DSE,[24] and other xDSE probes, where $x = 6$, 7,10, and 12 is the attachment point of the doxyl group[1] in solvents and mixtures in the literature. Values of the constants A_+^0 and $\partial A_+/\partial H$ for these spin probes are given in Table 2 of Part 1.[1] The same table gives values of the hydrodynamic radii of these probes. Some preliminary experiments are reported here by using spin probes CAT12 and CAT16. Calibration of these probes following the procedure detailed previously[12] yielded the following: $A_+^0 = 15.288 \pm 0.008$ G and $\partial A_+/\partial H = 1.437 \pm 0.010$ G for both spin probes.

A few experiments were performed (EPR only) with ^{15}N-substituted perdeuterated 17-doxyl stearic acid (^{15}N 17DSA) that was a kind gift from Dr. William Plachy. These data are presented because of the insight gained from the variation of pH in samples containing this acid; all other spin probes are either charged or not. A very limited amount of material was available so only a few experiments in SDS were possible. Likewise, only two samples were used to calibrate eq 9 yielding $A_0^0 = 20.21$ G and $\partial A_0/\partial H = 2.15$ G which are subject to larger, and at this point unknown, uncertainties than for the other spin probes. With this in mind, the absolute value of *H* is determined with less precision than normal; it is the differences in the results with and without added KOH that are interesting. Note that ^{15}N spin probes yield only two hyperfine lines, so A_0, the difference in their resonance fields, is measured instead of A_+. The larger hyperfine values for this spin probe are due to the larger nuclear magnetic dipole moment of ^{15}N. To compare the obtained values with ^{14}N spin probes, we divide by 1.403; thus, $A_0^0/1.403 = 14.40$ G and $\partial A_+/\partial H/1.403 = 1.53$ G, comparable to the other spin probes.

CHART 1: Structures of Nitroxide Spin Probes and Other Quenchers

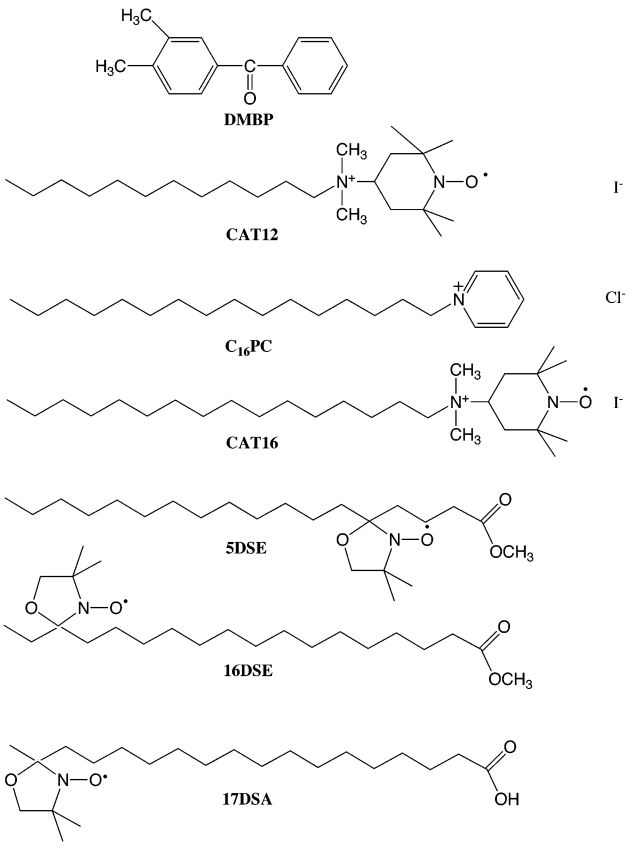

Departures of $H_{NO\bullet}$ from H_{shell}. Figure 3 shows a schematic one-quarter cross section of an SDS micelle as it grows from $N = 54$ to 104 maintaining a constant shell thickness. Three zones are depicted through which pyrene and NO• of 16DSE, 5DSE diffuse, respectively. Each zone extends symmetrically about the center of the micelle; only portions are shown for clarity. The broken lines represent schematic diffusive paths. There are many other possibilities for the diffusion zones, having different thicknesses, t_z, but we assume $t_z = t_s$ to avoid introducing adjustable parameters. Schematically, in Figure 3, the 5DSE zone remains within the shell as the micelle grows, while the pyrene zone remains displaced toward the inside. In Figure 3a, the 16DSE zone is displaced outward by a distance δ, and in Figure 3b, inward by δ. We use the convention that an outward displacement is positive and an inward, negative. To simplify the language, we speak of a spin probe being "farther out" or "farther in" than the polar shell to mean $\delta > 0$ or $\delta < 0$, respectively. We have anticipated the results in preparing Figure 3 to scale. The locations of 5DSE and 16DSE were determined in Part 1[1] and the location of pyrene is determined here. To distinguish the various values of δ, we adopt the following convention: a subscript identifies the moiety; e.g., δ_{16DSE} means the displacement of 16DSE from the ZOM. A location defined by the PPI carries in addition a superscript identifying the interaction probe, e.g., δ_{py}^{5DSE} means the position of pyrene with use of the known position of 5DSE as the interacting probe in the PPI and δ_{DMBP}^{py} means the position of DMBP with pyrene as the interacting probe.

To calculate $H_{NO\bullet}$, we assume that H_{shell} is uniform within the shell, $H = 0$ within the core, and $H = 1$ outside the shell.

Furthermore, the diffusion motion of NO• samples all portions of the zone with equal probability. See Figure 3 of ref 1. These assumptions could be relaxed at a cost of complexity that is not yet justified. For outward displacements of its zone, the average value of H sensed by NO• is easily shown to be the following:

$$H_{NO\bullet}^{theo} = \frac{[R_m{}^3 - (R_c + \delta)^3]H_{shell} + (R_m + \delta)^3 - R_m{}^3}{(R_m + \delta)^3 - (R_c + \delta)^3}; \quad 0 \le \delta \le t_s \quad (10)$$

where the shell thickness $t_s = R_m - R_c$. Equation 10 was reproduced incorrectly in Part 1;[1] however, the calculations and conclusions were based on the correct equation. For inward displacements,

$$H_{NO\bullet}^{theo} = \frac{[(R_m + \delta)^3 - R_c{}^3]H_{shell}}{(R_m + \delta)^3 - (R_c + \delta)^3}; \qquad 0 \ge \delta \ge -t_s \quad (11)$$

For the ZOM, $\delta = 0$ and both eqs 10 and 11 reduce to H_{shell}. Outside of the limits on δ in eqs 10 and 11, $H_{NO\bullet}^{theo} = 1$ or 0, respectively.

Hydrodynamic Description of Molecular Collisions in Micelles. A hydrodynamic theory of the quenching rate constant between molecules in micelles was recently introduced[25] and expanded.[26] Combining the Smoluchowski and the Stokes−Einstein equations yields the quenching rate constant

$$k_q = P_q P_c \frac{8 C_Q R T}{3000 \eta} = P_q P_c k_q^{SES} \quad (12)$$

where $R = 8.31 \times 10^7$ erg/K is the gas constant, T the absolute temperature, C_Q the concentration of the quencher, and η the viscosity (Poise). P_q is the probability of quenching upon collision of pyrene and a quencher and P_c is the probability that they occupy the same volume and thus may collide. Studies in bulk liquids show that P_q is of order unity for 5DSE and 16DSE; thus, we assume that $P_q = 1$ for nitroxides in micelles. In this paper, we refer to eq 12 as the Stokes−Einstein−Smoluchowski (SES) equation; the second equality in eq 12 defines the SES rate constant, k_q^{SES}.

In a micelle, the concentration C_Q is computed over the volume through which the quencher diffuses. Since k_q is the quenching rate constant due to one quencher, then, assuming for simplicity that this concentration is constant throughout the diffusion zone of the quencher and zero elsewhere, C_Q is the molar concentration of one molecule in the volume of the zone, V_q, thus

$$C_Q = \frac{10^{27}}{N_0 V_q} \quad (13)$$

where N_0 is Avogadro's number and V_q is in Å^3. The factor 10^{27} results from the conversion from Å^3 to liters. V_q is given by the first term in the denominator of eq 15, below, which reduces to V_{shell}, eq 3, if the quencher follows the ZOM. For values of δ_q found in this study, it is often not a good approximation to set $V_q = V_{shell}$ even though $t_z = t_s$, because they differ by 5−15% when δ_q is 13−37% of the shell thickness.

We simplify the model by assuming that the quencher and pyrene may be found with equal probability at any point within its respective zone of volume V_q or V_{py} and is not found outside those zones. Thus the probability that both molecules will be found in the region of overlap of volume $V_{overlap}$ is

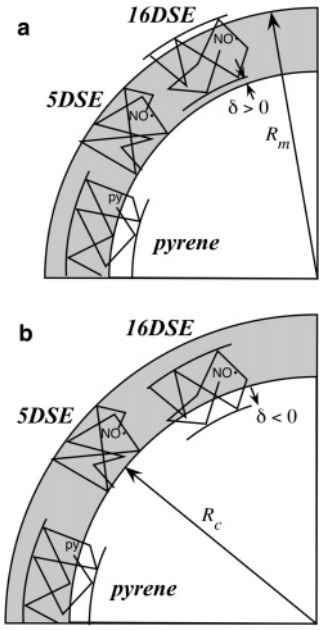

Figure 3. Schematic of the zones through which 5DSE, 16DSE, and pyrene diffuse. The thickness of the zones is equal to that of the shell, 4 Å. The zones extend concentrically around the micelle; only a portion is drawn for clarity. As the micelle grows from ***a*** to ***b*** by increasing the concentration of either the surfactant or added salt, 16DSE moves inward from residing outside the shell by $\delta > 0$ to inside by $\delta < 0$, while 5DSE maintains its position relative to the shell, following the ZOM. Pyrene is displaced inward from the polar shell, moving slightly as the micelle grows. The schematics are drawn to scale with shell thickness with (a) $N = 60$ and (b) $N = 120$. The displacements of the pyrene zone is that deduced from the PPI.

$$P_c = \frac{V_{overlap}{}^2}{V_q V_{py}} \quad (14)$$

Equation 14 can be quite complex if the quenchers and pyrene diffuse through different zone thicknesses. For the simplified model in which all $t_z = t_s$, eq 14 becomes

$$P_c = \frac{[(R_m + \delta_{py})^3 - (R_c + \delta_q)^3]^2}{[(R_m + \delta_q)^3 - (R_c + \delta_q)^3][(R_m + \delta_{py})^3 - (R_c + \delta_{py})^3]} \quad (15)$$

Equation 15 is valid for $[(R_m + \delta_{py}) - (R_c + \delta_q)] > 0$ and $|\delta_q - \delta_{py}| < t_s$, which turns out to be the case in this study. If $[(R_m + \delta_q) - (R_c + \delta_{py})] > 0$, then eq 15 holds with δ_q and δ_{py} interchanged. If $|\delta_q - \delta_{py}| \ge t_s$, then $P_c = 0$ (no overlap).

Microviscosity from EPR Measurements of the Rotational Correlation Time. The SES requires the viscosity of the medium through which the molecules diffuse. Fortunately, the same spin probes that serve as quenchers are ideal to measure the microviscosity. The rotational and translational motion of a moiety is conveniently modeled in terms of the Stokes−Einstein−Debye relation[27]

$$D_{trans} = \frac{kT}{6\pi R_h \eta} \quad (16)$$

$$D_{rot} = \frac{kT}{8\pi R_h{}^3 \eta} \quad (17)$$

where D_{rot} and D_{trans} are the rotational and translational diffusion constants of a spherical particle of radius R_h and η is the shear viscosity. Equations 16 and 17 apply to large spherical particles diffusing in homogeneous, continuous fluids; nevertheless, they are often used to describe molecular motion in solvents.[27] Equations 16 and 17 are only approximate, even in a bulk liquid;[28] nevertheless, they are useful because of the fact that the ratio D_{rot}/D_{trans} is constant for both bulk liquids and complex fluids and independent of temperature.[27] This means that departures from the simple hydrodynamic theory affect rotation and translation equally. Therefore, although η determined from eq 17 can be quantitatively different than the true shear viscosity, it is a convenient parameter allowing us to predict translational motion provided that we measure rotational motion. For flexible molecules such as 5DSE and 16DSE, the effective hydrodynamic radii of the diffusing NO• moieties are different from the radii of the entire molecules and are different from each other.[1] In a complex, inhomogeneous fluid such as a micelle, the viscosity is replaced by the microviscosity, η_{micro}. Outside the micelle, η_{micro} would have a value near the viscosity of water and, inside, would likely vary with position. We adopt the simplest approach and assume that η_{micro} is the value that emerges from the rotational correlation time of each spin probe. Values of the rotational correlation times for NO• moieties are deduced from the relative line heights of the three hyperfine lines, corrected for unresolved hyperfine structure as detailed previously.[12]

$$\tau_{rel} = \frac{4\pi\eta_{micro}R_h^3}{3kT} \tag{18}$$

Hydrodynamic radii are available in Table 2 of ref 1 for a number of flexible spin probes. The subscript rel refers to reorientation of the nitroxide group relative to a liquid at rest. To estimate the microviscosity from rotational correlation times measured in the laboratory frame of reference, τ_{lab}, the overall motion of the NO• group is modeled as a reorientation relative to the micelle as a unit with rotational correlation time τ_{rel} and an isotropic reorientation of the micelle as a whole with a characteristic time $\tau_{micelle}$. These reorientations are assumed to be independent, so

$$\frac{1}{\tau_{lab}} = \frac{1}{\tau_{rel}} + \frac{1}{\tau_{micelle}} \tag{19}$$

$\tau_{micelle}$ is computed from the Debye−Stokes−Einstein equation written as follows:

$$\tau_{micelle} = V_{micelle}\frac{\eta_{bulk}}{kT} \tag{20}$$

where η_{bulk} is the viscosity of the bath in which the micelle rotates. Further details on applying eqs 18−20 may be found in ref 29.

Materials and Methods

TRFQ measurements of pyrene quenched by 5DSE and 16DSE were performed with an Edinburgh Analytical Instruments FL900 lifetime measurement spectrometer as described in detail previously.[30] For quenchers Co(II), CAT16, CAT12, 3,4-dimethylbenzophenone (DMBP), and 5DSE a laser setup that has been described in detail[31] was used. We refer to the results obtained by these two methods as flash-lamp or laser data, respectively. The fluorescence decay curves were fitted to the following:[32,33]

$$f(t) = f(0)\exp\{-A_2t + A_3[\exp(-A_4t) - 1]\} \tag{21}$$

where

$$A_4 = k_q + k_-$$

$$A_2 = k_0 + \frac{k_qk_-\langle N_q\rangle}{A_4}$$

$$A_3 = \frac{k_q^2\langle N_q\rangle}{A_4^2}$$

where k_0 is the decay rate constant for pyrene in the absence of quencher, k_q the rate constant of quenching by a single quencher, k_- the exit rate constant of a quencher from the micelle, and $\langle N_q\rangle$ the average number of quenchers per micelle. A number of excellent reviews, e.g., refs 34 and 35, may be consulted for the assumptions involved in the derivation of eq 21 and its least-squares fit to experimental decay curves. For all quenchers except for Co(II) and Cu(II), k_- is negligible compared with k_q simplifying eq 21 considerably.

TRFQ has been an important method to estimate values of N from values of $\langle N_q\rangle$ and known surfactant and quencher concentrations, particularly useful at concentrations well above the cmc. The uncertainty in the value of N in any one experiment can easily reach ±10% due to uncertainties in the concentrations including $[SDS]_{free}$ as well as fitting uncertainties. Here, we are interested in k_q, which is rather insensitive to $\langle N_q\rangle$.

EPR spectra were obtained on an X-band Bruker 300ESP spectrometer equipped with a nitrogen gas-flow temperature controller. The temperature, measured with a thermocouple placed just above the active portion of the cavity, was stable within ±0.1 °C. Computer fits of the spectra yielded the line shapes, positions, and heights to high precision.[6] The collection and analysis of the EPR spectra have been described in great detail in previous publications[12,25] and the precision of the method has been discussed.[6]

Samples prepared for TRFQ employing spin probes as quenchers may be studied by EPR; nevertheless, care is needed because they contain higher concentrations of spin probe than $\langle N_q\rangle = 0.3$, the limit at which accurate values of EPR parameters may be obtained by spectral fitting. See Appendix C of ref 29. Above this concentration, the superposition of spectra due to more than one spin probe per micelle becomes too large to be properly interpreted by using presently available fitting software. The spectra may be doubly integrated to yield a quantity proportional to the spin probe concentration and compared with spectra obtained from a sample of known concentration. However, if the solvent is not water, another complication arises because the Q-factor of the cavity changes upon substitution of other solvents for water even if capillaries are used to house the samples. This means that a correction must be applied when comparing the intensities of a sample and a standard. In our experience, errors up to 30% can be incurred comparing samples in water and ethanol. In principle, the TRFQ samples could be diluted before measuring the EPR; however, they would need to be diluted with the same surfactant and salt concentrations to maintain the same value of N.

In addition to the materials used in the laser experiments previously described,[31] the following were purchased and used as received: $CoSO_4 \cdot 7H_2O$ (Merck, pro analysis; concentration determined by atomic absorption); DMBP (Aldrich 99%); and CAT12 and CAT16 (Molecular Probes). The materials used in the flash-lamp work have been described.[11]

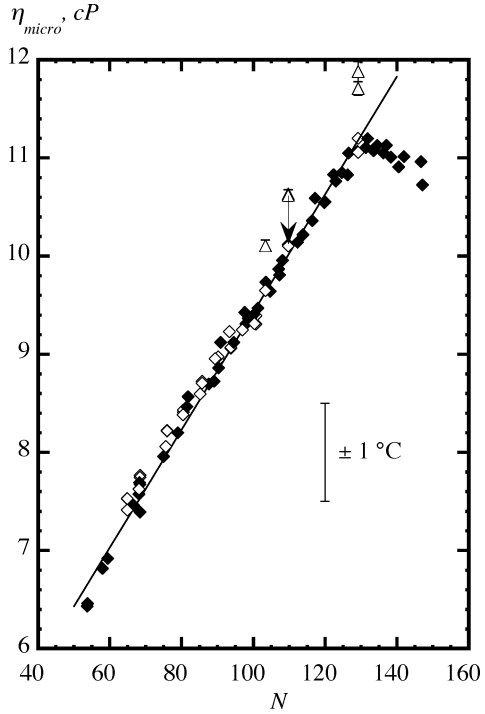

Figure 4. Microviscosity of SDS micelles as determined by 5DSE. Diamonds are computed from eqs 18−20 with use of the viscosity of SDS solutions (Table 1) for η_{bulk}. Filled and open diamonds correspond to add-salt and zero-salt samples. The data corresponding to four samples near $N = 103$, 110, and 129 were also computed with use of the viscosity of pure water for η_{bulk}; these are indicated by triangles. An arrow guides the eye showing the correction due to using the proper value of η_{bulk}. The isolated error bar indicates the change in η_{micro} due to a ±1 °C change in temperature. The line is a linear least-squares fit yielding $\eta_{5DSE} = 6.40 + 0.0600(N - N^0)$ in cP.

TABLE 1: Shear Viscosity of Aqueous SDS Solutions at 25 °C

[SDS], M	η_{bulk} no NaCl, cP	η_{bulk} add NaCl,[a] cP
0.025		0.915 (0.136 M)[b]
0.050	1.00[b]	
0.100	1.11[b]	1.03 (0.114 M)[b]
0.200	1.40[b]	1.17 (0.0856 M)[b]
0.300	1.73[b]	1.42 (0.0572 M)[b]
0.400	2.24[b]	1.86 (0.0285 M)[b]
0.500	2.65[b]	
0.600	3.52[c]	
0.965	7.98[c]	

[a] Concentration of added NaCl in parentheses. [b] Contraves LS 30 low-shear rheometer calibrated with MilliQ water. The viscosity was independent of shear rate over the range 1−100 rad/s. Error less than 1%. [c] CANNON PolyVisc Automatic Viscometer.

The shear viscosities of SDS solutions up to 500 mM were measured with a Contraves LS 30 low-shear rheometer calibrated with MilliQ water with an estimated error of less than 1%. The viscosity was independent of shear rate over the range 1−100 rad/s. Higher SDS concentrations were measured with a Cannon PolyVisc Automatic Viscometer.

Results

Bulk Viscosity. Table 1 gives values of the bulk viscosity of aqueous solutions of SDS in the presence and absence of salt. These data are in good agreement with literature values.[29]

Microviscosity. Figure 4 shows the microviscosity, η_{micro}, of SDS micelles as measured by 5DSE as a function of N. In this paper, N is computed from eq 5. Most of the data are taken from recent literature.[6,36] The open symbols were obtained from four separate experiments with newly prepared salt-free samples. The closed diamonds were obtained with low concentration SDS samples with added NaCl. The standard deviations from five or more spectra taken one after another on the same sample are about the size of the symbols or smaller in most cases. Different data points at the same value of N correspond to different runs with newly prepared samples. The dominant uncertainty from run to run is the temperature. This is illustrated by the isolated error bar that shows the uncertainty due to an uncertainty of ±1 °C in the temperature. Most of the data in Figure 4, denoted by diamonds, were computed from eqs 18−20, using the viscosity of the SDS solution (Table 1) for η_{bulk} in eq 20. This is a slight change from our procedure in recent papers where[10] we took η_{bulk} to be that of pure water. This correction is negligible for [SDS] < 50 mM but becomes more important at higher concentrations. To illustrate the difference, four of the data points near $N = 103$, 110, and 129 were computed in the previous approximate manner (triangles) while the diamonds directly below those points were computed from the same spectra with use of η_{bulk}. The solid line is a linear least-squares fit to all of the data (diamonds only) for $N < 130$ yielding $\eta_{micro} = 6.40 + 0.0600(N - N^0)$ in cP.

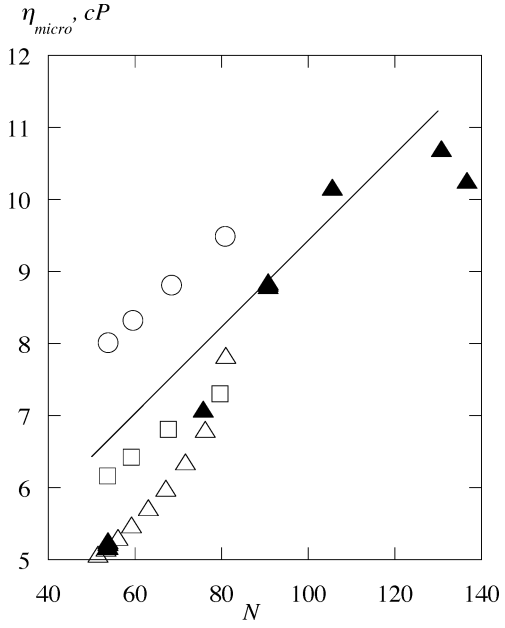

Figure 5. Microviscosity of SDS micelles as determined by CAT12, □; CAT16, ○; and 16DSE, △ (zero-salt) and ▲ (add-salt). The straight line is the fit to η_{5DSE} from Figure 4.

The proper treatment of the rotation of the micelle gives corrections that are insignificant in terms of obtaining the absolute value of η_{micro} and its use in the SES; however, it is significant in demonstrating that the rotational motion of NO• is dependent only on N; i.e., it is independent of the concentration of micelles which means that the rotational motion of NO• is not affected by the interactions between micelles. Figure 4 shows that η_{micro} conforms to a common curve to quite high surfactant concentrations provided that the micelle rotation is correctly modeled. Common curves of various experimental parameters derived from samples with and without added salt have been used to measure the degree of counterion dissociation, α, in recent papers.[6−9,11,23,37−39]

Figure 5 displays values of η_{micro} derived from measurements of 16DSE as a function of N in 25 mM SDS with added NaCl (filled triangles). Measurements of η_{micro} from spectra of 16DSE collected for a previous study[7] (no added salt) are shown by

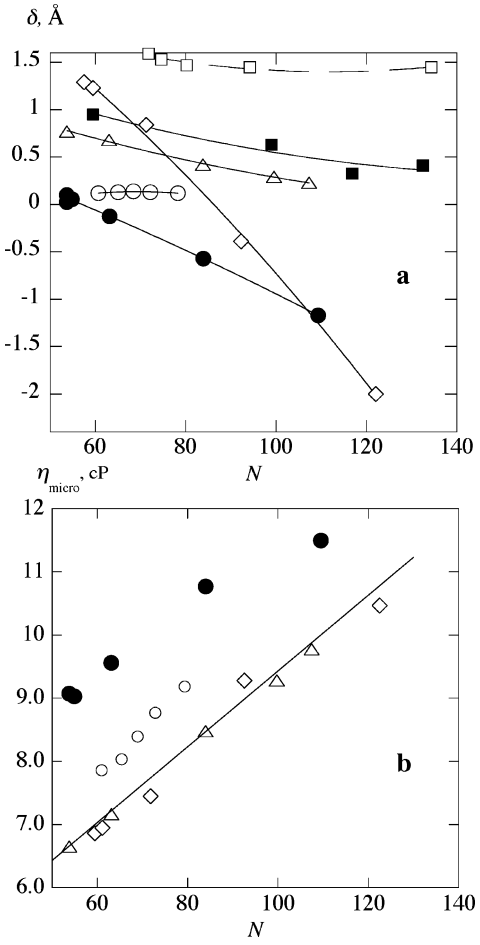

Figure 6. (a) Displacement of diffusion zones of doxylstearic acids and methyl esters 6DSE (○), 7DSE (△), 10DSE (●), 12DSE (◇), 17DSA (■), and 17DSA$^-$ (□). (b) Microviscosity of SDS micelles as determined by doxylstearic acid methyl esters.

open triangles. The straight line is the fit to 5DSE data in Figure 4. The open squares and open circles are derived from measurements of CAT12 (R_h = 4.7 Å) and CAT16 (R_h = 4.7 Å), respectively. Figure 6b displays values of η_{micro} derived from other spin probes.

Location of Spin Probes in SDS Micelles. For nitroxide spin probes, the PAI consists of comparing the theoretical value of $H^{theo}_{NO\bullet}$ with the experimental value of $H_{NO\bullet}$. This was the subject of Part 1 that described the procedure in detail.[1] Here, we shall briefly summarize, highlighting the small changes in the treatment of 5DSE and 16DSE dictated by now having more information. For given values of N, δ, and t_s, values of $H^{theo}_{NO\bullet}$ are uniquely determined by fixing V_{dry}, eq 7. Therefore, for any sample, theory and experiment may be brought into agreement by adjusting the value of V_{dry}. The fact that assuming the ZOM yielded $H^{theo}_{NO\bullet} = H_{NO\bullet}$ for 5DSE for all values of N in SDS as well as other sodium alkyl sulfate micelles with chain lengths 8, 9, 10, 11, 13, and 14 without any further adjustment of V_{dry} supported the model. See Part 1[1] for a critical discussion of this point. Further evidence that 5DSE followed the ZOM came from studies of ammonium dodecyl sulfate[23] where the same value of V_{dry}, when adjusted to account for the hydrogen bonding ammonium ion, correctly predicted the values of $H_{NO\bullet}$. Finally, the same value of V_{dry}, adjusted to include the volume of Br$^-$ in eq 8, predicted the correct values of $H_{NO\bullet}$ in DTAB,[2] again assuming the ZOM. Therefore, we assume that $H_{NO\bullet}$ for 5DSE, denoted by H_{5DSE}, is equal to H_{shell}. If it turns out that δ_{5DSE} is small but nonzero, all of the locations discussed here would need to be adjusted inward or outward by that amount. It is clear from eq 7 that the value of the adjustable parameter V_{dry} depends on the value assumed for the thickness of the shell, t_s. In past papers, due to our ignorance of the precise value of t_s, we have used t_s = 5 Å suggested from small-angle neutron scattering,[40] noting, however, that there is considerable uncertainty in this value. The present results shed further light on the question. If we persist in using t_s = 5 Å, we find values of $k_q > k_q^{SES}$ for 16DSE; i.e., $P_q > 1$, an unphysical result. Therefore we have adopted t_s = 4 Å in this work. We emphasize that this does not settle the issue; further results may necessitate further refinements.

The position of 16DSE was then determined by setting $H^{theo}_{NO\bullet} = H_{16DSE\bullet}$ and solving eq 10 or 11 for δ_{16DSE}, point by point, in a spread sheet as described in Part 1.[1] A plot of the results (not shown) is almost identical to those in Figure 4a of Part 1,[1] only a small adjustment is needed because t_s = 4 Å rather than 5 Å and because the results extend to higher values of N. Values of δ_{16DSE} again turn out to vary linearly with N as follows: $\delta_{16DSE} = 0.59 - 0.253(N - N^0)$, in angstroms, where N^0 = 49.5.

Figure 6a shows the position of NO• as a function of N for 6-, 7-, 10-, and 12DSE as well as 17DSA. The ionized probe, 17DSA$^-$, formed by adding 25 mM KOH is also represented in Figure 6a. Results for CAT12 and CAT16 appear below in Figure 8. As might be expected, 6DSE very nearly conforms to the ZOM while others show significant departures. The position of the diffusion zone of NO• for 12DSE is particularly sensitive, lying about 30% in the aqueous region and 70% in the polar shell at N = 57, while at N = 122 it lies about 50% in the polar shell and 50% in the core. As a practical matter, 12DSE would be more suitable as a probe to determine accurately if two values of N are the same in two samples, the cornerstone of measurements of α with EPR.[6] All of the NO• moieties of *x*DSE probes move inward as the micelle grows except for 5- and 6DSE. The squares are derived from limited data on 17DSA (filled) and 17DSA$^-$ (open). To plot the 17DSA$^-$ data, we have assumed that the abscissa is given by eq 5 with $C_{ad} = [Na^+] + [K^+]$. This is an approximation; nevertheless, despite some uncertainty in the value of N, it is clear that extracting the proton causes NO• to move outward. This is, perhaps, an unexpected result because the charged end of the molecule is well removed from NO•; however, this same effect has been observed[41] for 16DSA, where NO• was shown to experience higher polarity in SDS micelles upon addition of NaOH. The same author[41] reported no change in the hyperfine coupling constant of 5DSA, the acid form of 5DSE, upon addition of NaOH; however, the results were of lower precision than the present results. We avoid the acids when studying aggregates because the results are not as reproducible as those from the esters; nevertheless, it might be of interest to learn how to manipulate the position of NO• by varying pH.

Figure 6b displays values of η_{micro} derived from the 6-, 7-, 10-, and 12DSE employing the values of R_h in Table 2 of Part 1.[1] The straight line is the fit to the 5DSE data given in Figure 4. The microviscosities reported by 5DSE, 7DSE, and 12DSE are identical and that reported by CAT12 is very nearly equal to these (Figure 5). Values of η_{micro} reported by 6DSE and CAT16 (Figure 5) are somewhat larger, by 10DSE significantly larger, and by 16DSE, somewhat smaller than that reported by 5DSE. The averages of values of η_{micro} are given in Figure 10, below.

Loction of Pyrene with Use of 5DSE and 16DSE. Typical decay curves of pyrene fluorescence quenched by 5DSE, DMBP, and C_{16}PC have been published.[26] Decay curves due to 16DSE

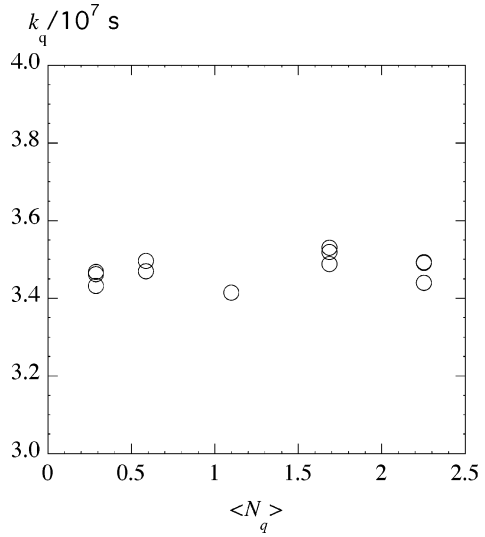

Figure 7. Quenching rate constant of pyrene by 5DSE as a function of the number of 5DSE molecules per micelle in 100 mM SDS at 25 °C.

Figure 8. Displacement of diffusion zones. (a) δ_{py} with the PPI with 5DSE (●), 16DSE (○), C_{16}PC(△), CAT12 (+), CAT16 (×). δ_q with the PAI for CAT12 (◆), CAT16 (◇), 5DSE (dashed line, Part 1);[1] and 16DSE (solid line, Part 1).[1] δ_q with the PPI fixing the position of pyrene, DMBP flash-lamp[42] (▲), Cu(II) laser (this work) (▽), and Cu(II) laser[44] (▼). (b) Detail of positions of pyrene with the PPI; solid line is the least-squares fit of δ_{py}^{5DSE} in part a. Note that + and ×, values of δ_{py}^{CAT12} and δ_{py}^{CAT16}, respectively, are set equal to δ_{py}^{5DSE} at $N = 53$ to find R_h; other values are from the PPI. Also note that the positions of pyrene determined from the PPI with C_{16}PC (△) assume that this quencher follows the ZOM in analogy with CAT16.

are very similar and all curves are well described by eq 21. One experiment was conducted as a function of the concentration of 5DSE. Figure 7shows the resulting values of k_q, demonstrating that it is constant with respect to quencher concentration. This result is expected if the Poisson distribution describes the distribution of quenchers among micelles and if the micelles have a small size dispersion.[34] Thus, for 5DSE, k_q is insensitive to uncertainties in the quencher concentration. Table 2 details the samples studied with 5DSE and 16DSE as quenchers and tabulates the measured values of k_q maintaining $\langle N_q \rangle \approx 1$. Some values are taken from the literature[26] and one datum is the average of the values in Figure 7. Values of N are computed from eq 5 and k_q^{SES} from eq 12 by using values of $\eta = \eta_{micro}$ taken from Figures 4 and 5. We define the experimental probability as follows:

$$P_c^{expt} = \frac{k_q}{P_q k_q^{SES}} \tag{22}$$

For each sample, values of δ_q (either 16DSE or 5DSE) are substituted into eq 15. Then, values of δ_{py}^{5DSE} or δ_{py}^{16DSE} in eq 15 are adjusted by trial and error in a spreadsheet until $P_c^{expt} = P_c$. Thus, in terms of the language developed in association with Figure 1, we employ the PAI to locate 16DSE and 5DSE (circles in Figure 1) and we use the PPI to locate pyrene. If we are successful, the location of pyrene will be unique. Figure 8 shows the results, wherein the location of pyrene determined from 5DSE (filled circles) corresponds rather well with those determined from 16DSE (open circles) at low values of N. At high values, they diverge somewhat but both still report the position of pyrene to be displaced somewhat toward the inside of the micelle. The solid line is the value of δ_{16DSE} and the dashed line is the value of δ_{5DSE} assumed to be zero because it adheres to the ZOM.

Figure 8 also shows the positions of CAT12 and CAT16 determined from the PAI and the position of pyrene as determined by the PPI with use of CAT12, CAT16, and C_{16}PC as described below. The locations of DMBP from flash-lamp results[42] and Cu(II) from laser results are also included. New laser data on DMBP are not plotted in Figure 8 for clarity; they fall almost exactly on top of the Cu(II) data. Of all of the quenchers considered in this paper, we only have full information available on 5DSE and 16DSE; for all of the others we must make at least one assumption in addition to those in the model. Table 3 summarizes these assumptions that are described in detail below. These assumptions were chosen to demonstrate possible approaches to locate molecules in self-aggregated systems.

The displacements of the diffusion zones from the polar shell are not dramatic: as SDS micelles grow from their value of about $N = 50$ at the cmc_0 to about 130 at the sphere-rod transition, 5DSE remains inside the shell, and 16DSE moves inward from lying about 10% in the aqueous phase and 90% in the polar shell to lying 60% in the shell and 40% in the core. When located by 5DSE or CAT16 pyrene moves outward from a zone lying about 63% in the polar shell, 37% in the core to one lying approximately 80% in the shell. DMBP and CAT16 follow the ZOM within experimental error, and C_{16}PC is assumed to do so. The largest displacement of all the probes is −2 Å (12DSE, Figure 6), which is 4% of the micelle diameter. Thus, all of the spectroscopic probes in Figure 8 predominantly occupy the polar shell. It is useful, when contemplating Figure 8, to refer to Figure 3 to avoid the impression that pyrene, for example, lies within the core.

Preliminary Results with Use of Other Spin Probes. The locations of CAT12 and CAT16, shown in Figure 8, were

TABLE 2: Quenching Rate Constants of Pyrene by 5DSE and 16DSE in SDS Micelles at 25 °C

spin probe	[SDS], mM	[NaCl], mM	N^a	k_q, 10^7 s^{-1}	η_{micro},[b] cP	SES k_q,[c] 10^7 s^{-1}	P_c^{expt} [d]	δ_{py},[e] Å
5DSE	25.0	0	53.8	4.10[f]	6.66	10.0	0.410	−1.44
5DSE	25.0	10.0	61.7	3.83[f]	7.14	8.60	0.446	−1.33
5DSE	100	0	68.4	3.48[h]	7.53	7.67	0.454	−1.30
5DSE	25.0	25.0	70.5	3.48[f]	7.66	7.40	0.470	−1.26
5DSE	25.0	49.3	80.5	3.32[f]	8.26	6.35	0.523	−1.11
5DSE	25.0	82.0	89.9	3.09[f]	8.83	5.55	0.556	−1.01
5DSE	100	63.0	90.7	3.01[i]	8.88	5.49	0.548	−1.04
5DSE	50.0	100	95.7	3.01[i]	9.17	5.15	0.585	−0.94
5DSE	25.0	126	99.3	3.00[f]	9.39	4.92	0.610	−0.87
5DSE	100	125	103	2.74[i]	9.63	4.69	0.585	−0.94
5DSE	25.0	191	110	2.79[f]	10.0	4.35	0.642	−0.80
5DSE	50.0	200	112	2.44[i]	10.1	4.23	0.576	−0.96
5DSE	25.0	271	119	2.66[f]	10.6	3.91	0.680	−0.70
5DSE	100	250	120	2.55[i]	10.6	3.88	0.657	−0.76
5DSE	25.0	355	127	2.46[f]	11.1	3.59	0.685	−0.687
5DSE	50.0	400	132	2.17[i]	11.4	3.42	0.634	−0.81
16DSE	25.0	0	53.8	4.61[f]	5.22	12.8	0.361	−1.10
16DSE	25.0	0	53.8	4.16[g]	5.22	12.8	0.326	−1.21
16DSE	25.0	10.0	61.7	4.23[f]	5.78	10.6	0.398	−1.20
16DSE	25.0	10.0	61.7	3.97[g]	5.78	10.6	0.371	−1.27
16DSE	25.0	25.0	70.5	4.00[f]	6.54	8.68	0.461	−1.25
16DSE	25.0	25.0	70.5	3.79[g]	6.54	8.68	0.434	−1.31
16DSE	25.0	34.0	74.6	3.73[g]	7.00		0.475	−1.31
16DSE	25.0	49.3	80.5	3.81[f]	7.59	6.91	0.552	−1.22
16DSE	25.0	82.0	89.9	3.61[f]	8.71	5.64	0.640	−1.20
16DSE	25.0	82.0	89.9	3.64[g]	8.71	5.64	0.652	−1.19
16DSE	25.0	126	99.3	3.58[f]	9.71	4.76	0.752	−1.18
16DSE	25.0	126	99.3	3.86[g]	9.71	4.76	0.810	−1.05
16DSE	25.0	191	110	3.69[f]	10.2	4.26	0.866	−1.20
16DSE	25.0	191	110	3.77[g]	10.2	4.26	0.885	−1.16
16DSE	25.0	271	119	3.60[f]	10.5	3.93	0.916	−1.35
16DSE	25.0	271	119	3.76[g]	10.5	3.93	0.956	−1.27
16DSE	25.0	355	127	3.44[f]	10.7	3.67	0.938	−1.60
16DSE	25.0	355	127	3.47[g]	10.7	3.67	0.944	−1.58

[a] Equation 5. [b] Equation 18. [c] Equation 12. [d] Equation 22. [e] Equation 15. [f] This work, flash-lamp. [g] This work, flash-lamp, second run. [h] Average value from Figure 7, laser. [i] Reference 26.

TABLE 3: Summary of Additional Assumptions to Derive Locations of Quenchers and Pyrene

	δ_q	η_{micro}	additional assumption(s)
5DSE	ZOM	eq 18	none
16DSE	eqs 10 and 11	eq 18	none
CAT12	eq 10	eq 18	find $R_h = 4.7 \pm 0.2$ Å $\delta_{py}^{CAT12} = \delta_{py}^{5DSE}$ at $N = 54$
CAT16	eqs 10 and 11	eq 18	find $R_h = 4.7 \pm 0.2_5$ Å $\delta_{py}^{CAT16} = \delta_{py}^{5DSE}$ at $N = 54$
C_{16}PC	unknown	unknown	$\eta_{micro} = \eta_{5DSE}$; ZOM by analogy with CAT16
DMBP	unknown	unknown	$\eta_{micro} = \eta_{5DSE}$; find δ_{DMBP}^{py}, using $\delta_{py} = \delta_{py}^{5DSE}$
Cu(II)	unknown	unknown	$\eta_{micro} = \eta_{5DSE}$; find $\delta_{Cu(II)}^{py}$, using $\delta_{py} = \delta_{py}^{5DSE}$
Co(II)	unknown	unknown	$\eta_{micro} = \eta_{5DSE}$; assume $\delta_{Co(II)} = \delta_{Cu(II)}$ find $P_{Co(II)}$

determined from the PAI. Laser studies of the fluorescence quenching of pyrene by these two nitroxides yielded typical curves, well described by eq 21, from which the values of k_q given in Table 4 were determined. Values of R_h from which values of η_{micro} may be computed from the EPR line-height ratios are not yet known for these spin probes. We estimate the values of R_h, employing a variation of the PPI at $N = 53$, by assuming that the position of pyrene is known and is equal to $\delta_{py}^{5DSE} = -1.45$ Å. Employing eqs 15 and 12 yields the value of η_{CAT12} and η_{CAT16} from which R_h may be computed. This results in $R_h = 4.7 \pm 0.2$ Å for both probes. The microviscosities are different as may be seen in Figure 5, but the hydrodynamic radii turn out to be the same. With this value of R_h in hand, we may then apply the PPI to CAT12 and CAT16 at other values of N in the same manner as with 5DSE and 16DSE. The results are given in Table 4 and Figure 8. Figure 8b shows greater detail. The straight line in Figure 8b is the linear fit to the 5DSE data in Figure 8a. Obviously, the fact that $\delta_{py}^{CAT12} = \delta_{py}^{CAT16} = \delta_{py}^{5DSE}$ at $N = 53$ is ensured by the procedure. However, it is significant that they remain approximately equal at other values; i.e., that the changes in position of pyrene as determined by the three spin probes are very similar. The open triangles in Figure 8b are discussed in the next section. The single error bar shows the uncertainty in δ_{py}^{5DSE} that would result from an uncertainty in R_h of ±5%.

Preliminary Locations Derived from Other Quenchers. The advantage of having the NO• group to locate a quencher using the PAI is lost when we use "traditional" quenchers such as DMBP, C_{16}PC, Cu(II), Co(II), and others. Furthermore, the microviscosity appropriate to each quencher is not available. Therefore, some assumptions, in addition to those inherent in the model, are required in order to proceed (Table 3). Of the many quenchers available in the literature, we shall consider in detail only DMBP, C_{16}PC,[26] and Cu(II),[31] because the data employing other quenchers were not often collected with the systematic variation of N in mind. We proceed by using η_{micro} as determined by 5DSE. In strategy 1 we assume that the location of pyrene is known to be equal to that defined by δ_{py}^{5DSE} to find the location of DMBP and Cu(II). Strategy 2 assumes that C_{16}PC follows the ZOM and finds the position of

TABLE 4: Quenching Rate Constants and Probe Locations of SDS Micelles at 25 °C.

quencher	N	η_{micro}, cP	k_q, 10^7 s^{-1}	k_q^{SES}, 10^7 s^{-1}[c]	δ_q, Å	δ_{py}, Å	H_{NO}
CAT16	53.8	8.01[a]	3.49[b]	8.42	−0.12[c]	−1.53[d]	0.683
CAT16	59.5	8.33[a]	3.17[b]	7.59	−0.07[c]	−1.48[d]	0.677
CAT16	68.4	8.81[a]	2.95[b]	6.54	0.02[e]	−1.30[d]	0.668
CAT16	80.8	9.49[a]	2.64[b]	5.44	0.14[e]	−1.07[d]	0.655
CAT12	53.8	6.16[a]	3.32[b]	10.5	0.28[e]	−1.47[d]	0.724
CAT12	59.5	6.43[a]	3.06[b]	9.45	0.34[e]	−1.40[d]	0.718
CAT12	68.4	6.81[a]	2.71[b]	8.18	0.42[e]	−1.28[d]	0.709
CAT12	80.8	7.30[a]	2.47[b]	6.88	0.51[e]	−1.09[d]	0.696
C_{16}PC	59.5	7.00[f]	4.18[g]	10.5	0[h]	−1.47[d]	
C_{16}PC	75.5	7.96[f]	3.57[g]	7.72	0[h]	−1.28[d]	
C_{16}PC	94.2	9.08[f]	3.13[g]	5.76	0[h]	−1.05[d]	
C_{16}PC	112	10.1[f]	2.78[g]	4.56	0[h]	−0.88[d]	
C_{16}PC	132	11.4[f]	2.25[g]	3.64	0[h]	−0.86[d]	
DMBP	75.1	7.93[f]	3.94[i]	6.89	−0.19	−1.17[j]	
DMBP	84.8	8.52[f]	3.56[i]	5.96	−0.14	−1.05[j]	
DMBP	90.9	8.88[f]	3.30[i]	5.49	−0.09	−0.984[j]	
DMBP	99.9	9.43[f]	3.02[i]	4.88	−0.04	−0.892[j]	
DMBP	108	9.91[f]	2.77[i]	4.43	0.02	−0.816[j]	
DMBP	116	10.4[f]	2.63[i]	4.05	0.03	−0.748[j]	
DMBP	123	10.8[f]	2.43[i]	3.76	0.09	−0.693[j]	
DMBP	126	11.0[f]	2.39[i]	3.63	0.08	−0.669[j]	
DMBP	133	11.4[f]	2.23[i]	3.40	0.13	−0.625[j]	
DMBP	53.8	6.66[f]	4.92[b]	10.0	−0.25	−1.45[j]	
DMBP	59.5	7.00[f]	4.49[b]	8.97	−0.21	−1.38[j]	
DMBP	68.4	7.53[f]	4.01[b]	7.67	−0.17	−1.27[j]	
DMBP	80.8	8.28[f]	3.59[b]	6.32	−0.14	−1.12[j]	
Cu(II)	53.8	6.66[f]	3.49[b]	7.27[k]	−0.21	−1.45[j]	
Cu(II)	59.5	7.00[f]	3.21[b]	6.50[k]	−0.19	−1.38[j]	
Cu(II)	68.4	7.53[f]	2.84[b]	5.51[k]	−0.14	−1.27[j]	
Cu(II)	80.8	8.28[f]	2.49[b]	4.49[k]	−0.10	−1.12[j]	
Cu(II)	68.4	7.53[f]	2.70[l]	5.51[k]	−0.07	−1.27[j]	
Co(II)	59.5	7.00[f]	0.68[b]	1.37[m]	−0.19[n]	−1.38[j]	

[a] Equation 18, $R_h = 4.7$ Å. [b] Laser data, this work. [c] Equation 11 with H_{NO}, in final column. [d] Equation 15. [e] Equation 10 with H_{NO}, in final column. [f] Computed from straight line, Figure 4. [g] Flash-lamp data, ref 26. [h] Assumed to conform to the ZOM in analogy with CAT16. [i] Flash-lamp data, ref 36. [j] Interpolated from 5DSE results for δ_{py}, Figure 8. [k] Equation 12 with $P_q = 0.72$. [l] Reference 44. [m] Equation 12 with $P_q = 0.15$ determined by setting $\delta_{Co(II)} = \delta_{Cu(II)}$. [n] Setting $\delta_{Co(II)} = \delta_{Cu(II)}$.

pyrene. A third strategy applied to Co(II) is described below. The rationale for strategy 2 is that CAT16 follows the ZOM very well and C_{16}PC is expected to be located similarly. Compare the structures of the two probes in Chart 1. We adjust the positions of either the quencher or pyrene until the experimental probability of quenching matches the theoretical.

Data for C_{16}PC taken from the literature[26] are given in Table 4. Because we have assumed the ZOM for this spin probe, we set $\delta_{C16PC} = 0$ and compute values of δ_{py}^{C16PC} given in column 7 of Table 4 and plotted (open triangles) in Figure 8. The locations of pyrene determined from 5DSE and CAT16 are remarkably similar, well within the experimental uncertainty over a wide range of N. A moment's thought shows that had we applied strategy 1 to C_{16}PC, taking the position of pyrene to be given by δ_{py}^{5DSE}, we would have found that C_{16}PC adheres very nearly to the ZOM.

New data employing DMBP derived from laser measurements are given in Table 4 together with some flash-lamp data gathered for ref 42 but not previously published. Taking $\delta_{py} = \delta_{py}^{5DSE}$ yields the location of DMBP as given in column 6 of Table 4 and plotted in Figure 8. Perhaps unexpectedly, DMBP very nearly adheres to the ZOM.

Quenching of pyrene fluorescence by Cu(II) has been extensively studied.[31,43−45] For typical decay curves, see, for example, Figures 2 and 3 of ref 31. Table 4 gives data from refs 44 and 31. In contrast to the quenchers in Chart 1, P_q departs significantly from unity for Cu(II). A quenching rate constant ($k_q = 5.3 \times 10^9$ M^{-1} s^{-1}) of 1-methylpyrene by Cu(II) in water has been reported by De Schryver and co-workers,[44] unfortunately without reporting the temperature. Those workers measured quenching rate constants for various metal ions and found no difference between pyrene and 1-methylpyrene. Grieser and Tausch-Treml[45] measured $k_q = (4.8 \pm 0.2) \times 10^9$ M^{-1} s^{-1} for Cu(II) quenching of pyrene at room temperature (20−23 °C). If we assume that the first group worked at 25 °C, then $P_q = 5.3 \times 10^9$ M^{-1} s^{-1}/7.4×10^9 M^{-1} s^{-1} = 0.72, where the denominator is computed from eq 12. Assuming the median temperature of 22 °C for the second group, $P_q = 4.8 \times 10^9$ M^{-1} s^{-1}/6.8×10^9 M^{-1} s^{-1} = 0.71. The similarity of these two results supports the supposition of 25 °C for De Schryver's[44] group.

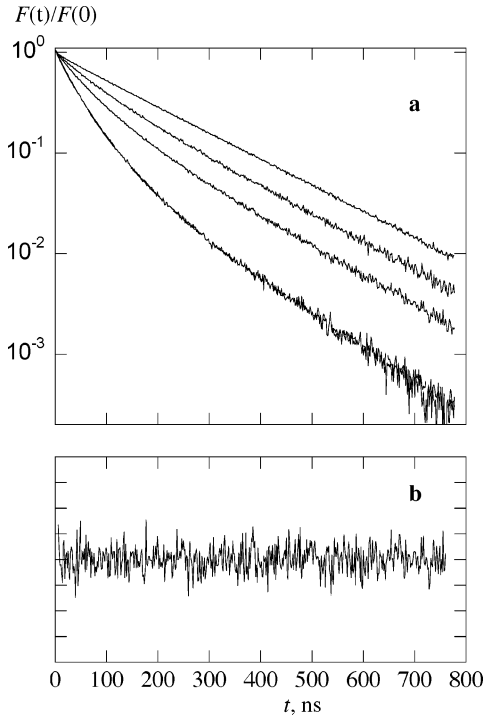

Figure 9. Fluorescence decay of pyrene quenched by Co(II) and residuals in 50 mM SDS at 25 °C. The four curves in part a correspond to the number of Co(II) ions per micelle $N_q = 0$, 0.57, 1.15, and 2.3, respectively.

Following strategy 1, we suppose that $\delta_{py} = \delta_{py}^{5DSE}$ and solve eq 15 for $\delta_{Cu(II)}$ assuming that $P_q = 0.72$. These are given in column 6 of Table 4 and plotted in Figure 8, showing that Cu(II) nearly adheres to the ZOM. In this case, we might have anticipated this result because of the electrostatic attraction between the headgroups and Cu(II).

Figure 9 shows pyrene fluorescence decay curves (laser) quenched by Co(II) in 50 mM SDS without added salt, which may be compared with Figure 3b of ref 43. However, the authors of the previous report[43] did not analyze the data in terms of eq 21. The fit and excellent residuals show that these decay curves are well fit by eq 21, yielding $k_q = (0.68 \pm 0.04) \times 10^7$ s^{-1}. De Schryver and co-workers[44] reported $k_q = 0.54 \times 10^7$ s^{-1} for 100 mM SDS from which we estimate $k_q = 0.59 \times 10^7$ s^{-1} for 50 mM SDS, somewhat smaller than our value. Here, we apply a third strategy using the PPI, reasoning that the positions of Cu(II) and Co(II) are probably not much different. By fixing the position of Co(II) at the position of Cu(II) and the position

of pyrene to be $\delta_{py} = \delta_{py}^{5DSE}$, we compute $P_q = 0.15$, about a factor of 4.7 less than that for Cu(II).

Discussion

The position of the diffusion zone of pyrene, when derived from 5DSE, resides approximately 60% inside the polar shell and 40% into the core at $N = 53$ and moves outward to a 80%: 20% ratio as the micelle grows to $N = 130$, near the sphere−rod transition. Under the plausible assumption that C_{16}PC follows the ZOM because CAT16 does, the positions of pyrene determined from C_{16}PC are very similar to those determined from 5DSE. At low values of N, the changes in the position of pyrene determined from CAT16 and CAT12 are very similar to those determined from 5DSE. At low values of N the values of δ_{py}^{16DSE} are in satisfactory agreement with δ_{py}^{5DSE}. Summarizing, the position of pyrene as determined by 4 spin probes other than 5DSE is the same as that determined from the benchmark, 5DSE, within ±0.4 Å. At higher values, 5DSE and C_{16}PC report the same position of pyrene, but that derived from 16DSE diverges by about 0.8 Å. In view of the uncertainties discussed below, the consistency of the location of pyrene is satisfactory.

It is important to note that the fact that 16DSE moves inward significantly as the micelle grows allows us to conclude that pyrene is farther into the micelle and not farther out; i.e., $\delta_{py} < 0$ and not $\delta_{py} > 0$. All of the other quenchers considered here depart very little from the ZOM. From those quenchers alone, we would not be able to conclude that $\delta_{py} < 0$; they could all be explained with $\delta_{py} > 0$. This is an ambiguity reminiscent of the dashed rectangle of Figure 1. Note that the conclusion that pyrene is located farther into the micelle than 5DSE could be reached simply from the raw 16DSE k_q data without any reference to the SES. The fact that 16DSE moves inward as N increases and the value of k_q due to 16DSE increases relative to that of 5DSE is sufficient to draw this conclusion. Obviously, further confirmation of the location of pyrene is desirable in its own right and to lend further support to the model. Fortunately, other quenchers that depart significantly from the ZOM are available, for example, 12DSE (Figure 6a). This quencher would provide a very severe test of the models in this paper, because we may, a priori, predict the values of k_q because values of the microviscosity and δ_{12DSE} are available.

The model rests upon two main assumptions: (a) that the core−shell model and the simple formulation of the hydration of the polar shell, Figure 2 and eq 3, are valid and (b) the SES is valid. Each of these main assumptions involves a number of others.

We have critically discussed assumption (a) in recent papers[2,8,13,23,24] and have accumulated enough data to have confidence in eqs 7 and 8. We have already pointed out that values of H_{5DSE} are correctly predicted in a wide variety of micelles over a wide range of values of N. Briefly summarizing other evidence, substituting Na^+ for Li^+ in dodecyl sulfate micelles gives the same value of H_{shell} at the same value of N despite the fact that very different values of C_{aq} are required to produce a given value of N.[13] This supports the assumption that the waters of hydration of these ions do not contribute to V_{dry} differently than the "free" waters. Thus, in eq 8, V_{ci} is that of the bare ion for these ions and is negligible. Substituting NH_4^+ for Na^+ in dodecyl sulfate micelles gives the same value of H_{shell} at the same value of N when the nonnegligible value of V_{ci} for the ammonium ion is taken into account and a small correction for the fact that NH_4^+ forms hydrogen bonds.[23] In dodecyltrimethylammonium micelles, substituting Br^- for Cl^- gives the same value of H_{shell} at the same value of N, again with different values of C_{aq} required to produce the same value of N, when the small difference in V_{ci} is taken into account.[8] In this case, V_{ci} is not negligible. When large sugar-based headgroups are inserted into SDS, the expelled volume of water is near that of V_{hg} for the headgroup as calculated from molecular models.[24] Particularly encouraging is the fact that H_{shell} calculated a priori for DTAB from eqs 6 and 7 with use of values appropriate for SDS with only the value of V_{ci} changed to that for Br^- are in agreement with experiment.[2] In a series of experiments in dodecyl sulfate micelles, progressively larger tetraalkyl ammonium counterions were substituted for the alkali metal ions.[9,10,46,47] Unfortunately, the spin probe 16DSE was used for that work at a time that we did not realize that it was not well described by the ZOM. Thus, values of H_{shell} were not measured, rather those of H_{16DSE}. We do not have the necessary location information for 16DSE in those micelles, thus a quantitative affirmation of eqs 7 and 8 is not yet possible. Nevertheless, their basic truth was reaffirmed because the larger the counterion, the smaller the value of H_{16DSE}.[9,10,46,47]

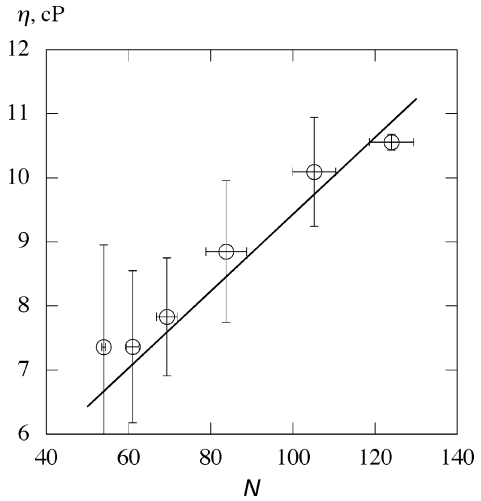

Figure 10. Average values and standard deviations of the microviscosities of SDS micelles determined by all spin probes except for 5DSE (○); straight line, fit of the microviscosity determined from 5DSE. The horizontal error bars are the standard deviations of the values of N binned together to compute the averages.

Turning to assumption (b), combining eqs 12, 13, and 22 and evaluating the constants give the following for the experimental probability of collision:

$$P_c^{expt} = \frac{k_q}{P_q} \frac{V_q \eta_{micro}}{(3.68 \times 10^{10})T} \qquad (23)$$

In eq 23, V_q is in Å^3 and η_{micro} in cP. After finding k_q from the experiment and fixing P_q and T, P_c^{expt} is determined by the product $V_q\eta_{micro}$. The relative positions of the two probes follow from P_c^{expt}. Therefore, only V_q and η_{micro} enter into the computation of the relative positions of the two probes once t_z is chosen.

We have argued that it is preferable to use values of η_{micro} appropriate to each quencher, when it is available. This is because η_{micro} is, in effect, a parameter that relates the required translational motion to the measurable rotational motion. An alternative would be to assume that an SDS micelle is characterized by a given value of η_{micro} at a given value of N and that this value is independent of the location of the probe. In this view, the differences in values of η_{micro} would be interpreted as uncertainties. Figure 10 shows the mean values and standard deviations of values of η_{micro} given in Figures 4,

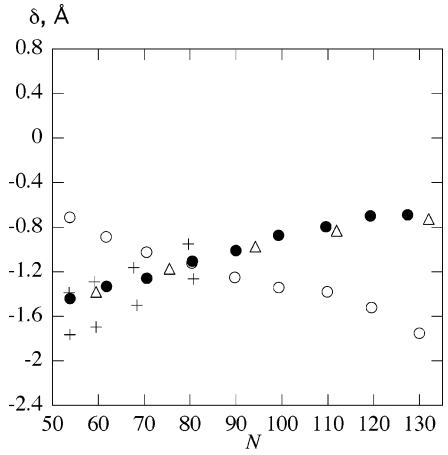

Figure 11. The displacement of the diffusion zone of pyrene in SDS micelles as determined by the PPI with various quenchers, recalculated by using the average values of the microviscosity, Figure 10, rather than individual microviscosities, at 25 °C. The symbols are the same as in Figure 8.

5, and 6b. The straight line is the fit to 5DSE data taken from Figure 4. We see that the mean values are near those derived from 5DSE. The standard deviations vary from about 20% at low values of N to about 2% at high values. A 1.0 °C error in T would introduce another ±6% error into η_{micro}. Therefore, a significant fraction of the uncertainties in Figure 10 are due to these two factors. To give an idea of how uncertainties in η_{micro} propagate into uncertainties in δ_{py}, we have added an error bar to Figure 8b showing the uncertainty in δ_{py}^{5DSE} due to a ±15% error in η_{micro}, propagated from a ±5% uncertainty in the value of R_h. To show the overall effect of using mean values of η_{micro} instead of individual values, we have recalculated the values of δ_{py} derived from various quenchers; these are presented in Figure 11. Comparing Figure 11 with Figure 8 shows that results are more consistent with use of individual values; nevertheless, either approach gives satisfactory results given the simplicity of the model. An excellent further test of whether individual values of η_{micro} are more appropriate would be provided by using 10DSE to quench pyrene because, as Figure 6b shows, the microviscosities derived from this spin probe are significantly larger than all of the others.

Values of η_{micro} in micelles estimated from various techniques vary widely in a literature that is vast and controversial.[48] For a recent discussion of the dependence of the results on the probe employed and relevant references see ref 48. Even the concept of microviscosity has been criticized.[49−51] In particular, microviscosities derived from the probe dipyrenylpropane[52−54] are considerably larger than those reported by spin probes. Olea and Thomas[28] applied eq 12 to some measurements of the quenching of pyrene to deduce values of η_{micro} that were consistent with the larger values. They[28] assumed a region of diffusion of pyrene and the quencher that is considerably different from those found in this study and implicitly assumed full overlap to derive their results. In other words, Olea and Thomas[28] assumed the information that we are trying to ascertain and then deduced values of η_{micro}. Stilbs et al.[55] carried out a careful study of the deuterium NMR spin relaxation of *trans*-Decalin-d_{18} in a variety of micelles overcoming a number of previously encountered difficulties. They arrived at estimates of η_{micro} by comparing the rotational correlation times with those in bulk hydrocarbons. They found that $\eta_{micro} = 3.4$ cP in DTAB and 4.3 cP in SDS at 35 °C. Carrying out measurements with 16DSE at 35 °C, we find 4.2 and 4.3 cP for 25 mM DTAB and SDS, respectively. Stilbs et al.[55] emphasized the point that the values of η_{micro} are model dependent as are the values reported in this paper; thus, the rather good agreement between two very different probes with entirely different methods tends to support both methods. Also encouraging is the fact that *trans*-Decalin is a rigid molecule while the spin probes are flexible. The obvious advantage to the NMR approach and our approach is that estimates of η_{micro} are derived from measurements that require no assumptions involving eq 12.

Values of V_q are dominated by the choice of the zone thickness; indeed, for SDS micelles, V_q is nearly proportional to t_z. We have restricted $t_z = t_s$; however, even a 0.5 Å change in t_z yields a 13% change in V_q that enters explicitly into the calculation of P_c. Furthermore, changes in t_z lead to changes in the values of P_c that are rather complicated, and enter implicitly through the term $V_{overlap}$.

In view of these estimates, it is remarkable indeed that the data fit the model as well as they do employing the same value of the thickness of all diffusion zones, both pyrene and the quenchers.

An obvious criticism of the model is the use of the SES for the quenching of pyrene by a quencher. Inherent in the model is that a contact collision between the two molecules is required to produce quenching. Such a model is easy to visualize for spin exchange interactions between two nitroxide spin probes, where the reaction center of NO• is rather localized within the orbital of the unpaired spins, but not so easy with a large molecule like pyrene. The SES does work well for pyrene quenched by various quenchers in a bulk liquid.[26] The consistency achieved in locating pyrene in these experiments supports the working hypothesis that it works well in SDS micelles. It is easy to design many experiments that will solidify our understanding by using some of the quenchers considered in this paper and undoubtedly many others.

Future Possibilities. The reader may have noticed that an important source of information could be obtained by measuring the spin exchange frequency between nitroxide spin probes. In the schematic of Figure 1, this would correspond to applying the PPI to moieties *A* and *B* and could severely test the model. If these nixtroxides are identical, then P_c is obviously unity and the focus would be on correct values of η_{micro} and V_q. If they were different, we could test the locations of each against the relative locations resulting from application of the PPI. The experiment would have to be carried out by using ^{14}NO• in one probe and ^{15}NO• in the other so that the signals could be separated. These experiments are easy to perform, and a number of publications have appeared;[56−58] however, there are three problems to overcome in their interpretation. First, the separation of spectra from singly occupied, doubly occupied, etc. micelles must be done by nonlinear least-squares fitting; i.e., software will have to be developed. Second, not only spin exchange but also dipolar interactions can affect the spectra depending on the conditions.[59] Separation of these two interactions is now possible, in principle,[60−62] in bulk solvents, but would require careful analysis of the separate components of the spectrum. A problem could arise due to spin statistics in the spin exchange process. Finally, the complicated spectra due to a mixture of ^{14}NO• and ^{15}NO• spin probes would also require software. There is no reason to believe that all three problems cannot be overcome, permitting this valuable tool to be employed.

It would be an important step forward to learn to apply the PAI to quenchers other than nitroxides to avoid an additional assumption as outlined in Table 3. The well-known dependence of the fluorescence intensities in the first and third bands would be such a step if the problems associated with reproducibility

and lack of a solid theory[12,43] could be overcome. If optical spectra of C_{16}PC or DMBP could be reproducibly correlated with *H*, this additional information would allow us to independently locate pyrene using the PPI. A similar innovation would be to learn to locate arenediazonium salts in aggregates spectroscopically. This might permit an independent approach to verify the model by using chemical trapping of water[63] as a measure of *H*.

Conclusions

The PAI applied to nitroxide spin probes shows that 5DSE, 6DSE, and CAT16 adhere to the zero-order model in SDS; i.e., the NO• moiety of each probe diffuses through the polar shell as *N* varies. Positively charged CAT12, neutral 17DSA, and 7DSE are displaced outward at low values of *N*, moving inward as *N* increases. 10DSE begins within the polar shell at low values of *N* and moves inward, while 12DSE begins outside the shell and moves inward by a significant amount. These results will permit the design of future experiments to test the PPI model. Employing the PPI, with reasonable assumptions, shows that Cu(II) and DMBP adhere approximately to the ZOM. Pyrene, located by the PPI, using 5DSE and C_{16}PC, is displaced toward the interior of the micelle by about 35% of the polar shell thickness at low values of *N* and moves outward to about a 20% displacement toward the interior near the sphere−rod transition at $N = 130$. Fixing the location of pyrene at $N = 53$ to calibrate the hydrodynamic radii of CAT12 and CAT16 shows that the rate of outward movement of pyrene as a function of *N* is the same as that derived from 5DSE and C_{16}PC. More consistent results are obtained for the location of pyrene as measured from various quenchers if the microviscosity is treated as a parameter connecting the rotational and translational motions of the moieties rather than an intrinsic property of the micelle, although either view gives satisfactory results.

Acknowledgment. Financial support from the NIH (S06 GM 48680) is gratefully acknowledged. We also wish to thank a referee who brought ref 55 to our attention.

References and Notes

(1) Lebedeva, N. V.; Bales, B. L. *J. Phys. Chem. B* **2006**, *110*, 9791.
(2) Lebedeva, N. V.; Bales, B. L. *J. Phys. Chem. B* **2006**, *110*, 9800.
(3) Tanford, C. *The Hydrophobic Effect*: *Formation of Micelles and Biological Membranes*., 2nd ed.; Wiley-Interscience: New York, 1980.
(4) Quina, F. H.; Nassar, P. M.; Bonilha, J. B. S.; Bales, B. L. *J. Phys. Chem.* **1995**, *99*, 17028.
(5) Sasaki, T.; Hattori, M.; Sasaki, J.; Nukina, K. *Bull. Chem. Soc. Jpn.* **1975**, *48*, 1397.
(6) Bales, B. L. *J. Phys. Chem. B* **2001**, *105*, 6798.
(7) Bales, B. L. An Aggregation Number-Based Definition of the Ionization of a Micelle. Demonstration with TRFQ, SANS, and EPR. In *Magnetic Resonance in Colloid and Interface Science*; Fraissard, J., Lapina, O., Eds.; Kluwer Academic Publishers: Dordrecht, The Netherlands, 2002; Vol. 76, p 277.
(8) Bales, B. L.; Zana, R. *J. Phys. Chem. B* **2002**, *106*, 1926.
(9) Bales, B. L.; Tiguida, K.; Zana, R. *J. Phys. Chem. B* **2004**, *108*, 14948.
(10) Bales, B. L.; Benrraou, M.; Tiguida, K.; Zana, R. *J. Phys. Chem. B* **2005**, *109*, 7987.
(11) Lebedeva, N. V.; Shahine, A.; Bales, B. L. *J. Phys. Chem. B* **2005**, *109*, 19806.
(12) Bales, B. L.; Messina, L.; Vidal, A.; Peric, M.; Nascimento, O. R. *J. Phys. Chem. B* **1998**, *102*, 10347.
(13) Bales, B. L.; Shahin, A.; Lindblad, C.; Almgren, M. *J. Phys. Chem. B* **2000**, *104*, 256.
(14) Ramachandran, C.; Pyter, R. A.; Mukerjee, P. *J. Phys. Chem.* **1982**, *86*, 3198.
(15) Mukerjee, P.; Ramachandran, C.; Pyter, R. A. *J. Phys. Chem.* **1982**, *86*, 3189.
(16) Pyter, R. A.; Ramachandran, C.; Mukerjee, P. *J. Phys. Chem.* **1982**, *86*, 3206.
(17) Schwartz, R. N.; Peric, M.; Smith, S. A.; Bales, B. L. *J. Phys. Chem. B* **1997**, *101*, 8735.
(18) Griffith, O. H.; Dehlinger, P. J.; Van, S. P. *J. Membr. Biol.* **1974**, *15*, 159.
(19) Knauer, B. R.; Napier, J. J. *J. Am. Chem. Soc.* **1976**, *98*, 4395.
(20) Reddock, A. H.; Konishi, S. *J. Chem. Phys.* **1979**, *70*, 2121.
(21) Abe, T.; Tero-Kubota, S.; Ikegami, Y. *J. Phys. Chem.* **1982**, *86*, 1358.
(22) Jackson, S. E.; Smith, E. A.; Symons, M. C. R. *Discuss. Faraday Soc.* **1978**, *64*, 173.
(23) Tcacenco, C. M.; Zana, R.; Bales, B. L. *J. Phys. Chem. B* **2005**, *109*, 15997.
(24) Bales, B. L.; Howe, A. M.; Pitt, A. R.; Roe, J. A.; Griffiths, P. C. *J. Phys. Chem. B* **2000**, *104*, 264.
(25) Bales, B. L.; Ranaganathan, R.; Griffiths, P. C. *J. Phys. Chem. B* **2001**, *105*, 7465.
(26) Ranganathan, R.; Vautier-Giongo, C.; Bales, B. L. *J. Phys. Chem. B* **2003**, *107*, 10312.
(27) Kovarskii, A. L.; Wasserman, A. M.; Buchachenko, A. L. *J. Magn. Reson.* **1972**, *7*, 225.
(28) Olea, A. F.; Thomas, J. K. *J. Am. Chem. Soc.* **1988**, *110*, 4494.
(29) Bales, B. L.; Stenland, C. *J. Phys. Chem.* **1993**, *97*, 3418.
(30) Ranganathan, R.; Peric, M.; Bales, B. L. *J. Phys. Chem. B* **1998**, *102*, 8436.
(31) Bales, B. L.; Almgren, M. *J. Phys. Chem.* **1995**, *99*, 15153.
(32) Infelta, P. P.; Grätzel, M.; Thomas, J. K. *J. Phys. Chem.* **1974**, *78*, 190.
(33) Tachiya, M. *Chem. Phys. Lett.* **1975**, *33*, 289.
(34) Grieser, F.; Drummond, C. J. *J. Phys. Chem.* **1988**, *92*, 5580.
(35) Gehlen, M. H.; De Schryver, F. C. *Chem. Rev.* **1993**, *93*, 199.
(36) Ranganathan, R.; Peric, M.; Medina, R.; Garcia, U.; Bales, B. L.; Almgren, M. *Langmuir* **2001**, *17*, 6765.
(37) Vautier-Giongo, C.; Bales, B. L. *J. Phys. Chem. B* **2003**, *107*, 5398.
(38) Bales, B. L.; Zana, R. *Langmuir* **2004**, *20*, 1579.
(39) Bales, B. L.; Benrraou, M.; Zana, R. *J. Phys. Chem. B* **2002**, *106*, 9033.
(40) Cabane, B.; Duplessix, R.; Zemb, T. *J. Phys.* **1985**, *46*, 2161.
(41) Yoshioka, H. *J. Am. Chem. Soc.* **1979**, *101*, 28.
(42) Ranganathan, R.; Tran, L.; Bales, B. L. *J. Phys. Chem. B* **2000**, *104*, 2260.
(43) Konuk, R.; Cornelisse, J.; McGlynn, S. P. *J. Phys. Chem.* **1989**, *93*, 7405.
(44) Dederen, J. C.; Van der Auweraer, M.; De Schryver, F. C. *J. Phys. Chem.* **1981**, *85*, 1198.
(45) Grieser, F.; Tausch-Treml, R. *J. Am. Chem. Soc.* **1980**, *102*, 7258.
(46) Benrraou, M.; Bales, B. L.; Zana, R. *J. Phys. Chem. B* **2003**, *107*, 13432.
(47) Zana, R.; Benrraou, M.; Bales, B. L. *J. Phys. Chem. B* **2004**, *108*, 18195.
(48) Dutt, G. B. *J. Phys. Chem. B* **2004**, *108*, 3651.
(49) Henderson, C. N.; Sellinger, B. K.; Watkins, A. R. *J. Photochem.* **1981**, *16*, 215.
(50) Hare, F.; Amiell, J.; Lussan, C. *Biochim. Biophys. Acta* **1979**, *555*, 388.
(51) Maiti, N. C.; Krishna, M. M. G.; Britto, P. J.; Periasamy, N. *J. Phys. Chem. B* **1997**, *101*, 11051.
(52) Turley, W. D.; Offen, H. W. *J. Phys. Chem.* **1985**, *89*, 2933.
(53) Turley, W. D.; Offen, H. W. *J. Phys. Chem.* **1986**, *90*, 1967.
(54) Zana, R. *J. Phys. Chem. B* **1999**, *103*, 9117.
(55) Stilbs, P.; Walderhaug, H.; Lindman, B. *J. Phys. Chem.* **1983**, *87*, 4762.
(56) Aizawa, M.; Komatsu, T.; Nakagawa, T. *Bull. Chem. Soc. Jpn.* **1979**, *52*, 980.
(57) Aizawa, M.; Komatsu, T.; Nakagawa, T. *Bull. Chem. Soc. Jpn.* **1980**, *53*, 975.
(58) Shirahama, K.; Tohdo, M.; Murahashi, M. *Colloid Polym. Sci.* **1984**, *262*, 978.
(59) Molin, Y. N.; Salikhov, K. M.; Zamaraev, K. I. *Spin Exchange. Principles and Applications in Chemistry and Biology*; Springer-Verlag: New York, 1980; Vol. 8.
(60) Bales, B. L.; Peric, M. *J. Phys. Chem. B* **1997**, *101*, 8707.
(61) Bales, B. L.; Peric, M. *J. Phys. Chem. A* **2002**, *106*, 4846.
(62) Bales, B. L.; Peric, M.; Dragutan, I. *J. Phys. Chem. A* **2003**, *107*, 9086.
(63) Soldi, V.; Keiper, J.; Romsted, L. S.; Cuccovia, I. M.; Chaimovich, H. *Langmuir* **2000**, *16*, 59.